A Composite Velocity Procedure for the Compressible Navier-Stokes Equations

P. K. Khosla* and S. G. Rubin†
University of Cincinnati, Cincinnati, Ohio

A new boundary-layer relaxation procedure is presented. In the spirit of the theory of matched asymptotic expansions, a multiplicative composite of the appropriate velocity representations for the inviscid and viscous regions is prescribed. The resulting equations are structured so that far from the surface of the body the momentum equations lead to the Bernoulli relation for the pressure, while the continuity equation reduces to the familiar compressible potential equation. Close to the body surface, the governing equations and solution techniques are characteristic of those describing interacting boundary layers, although the full Navier-Stokes equations are considered here. Laminar flow calculations for the subsonic flow over an axisymmetric boattail simulator geometry are presented for a variety of Reynolds and Mach numbers. A strongly implicit solution method is applied for the coupled velocity components.

Introduction

ONE of the major differences between solution techniques for the Navier-Stokes equations and those for either inviscid potential flow or boundary-layer flow is the treatment of the continuity equation. For inviscid flow, a potential function is determined entirely from this equation. The pressure is then obtained from the integrated momentum or Bernoulli equation. For boundary layers, the axial momentum and continuity equations determine the velocities. The pressure is obtained from the inviscid solution, i.e., momentum equations. On the other hand, typical Navier-Stokes solvers, in effect, use the continuity equation to obtain the density (or pressure), and the velocities result solely from the momentum equations. For large Reynolds number (Re) flows, it would appear that such a procedure is at variance with both the asymptotic inviscid and boundary-layer theories.

In the present paper, a boundary-layer relaxation procedure based on a new composite-velocity formulation for the compressible Navier-Stokes equations is described. In particular, the laminar subsonic flow over a boattail geometry is used as a prototype problem in order to test the applicability of the composite velocity formulation. The procedure has also been developed independently for incompressible flow.[1,2] Unlike typical Navier-Stokes procedures that differ significantly from their compressible flow counterparts, the present developments are essentially identical in both cases. Therefore, the compressible solution procedure can be applied in the limit Mach number $\to 0$ to recover identically the incompressible solutions.

The equations are written in a body-fitted orthogonal coordinate system so that arbitrary geometries can be treated. The formulation is directly extendable to three-dimensional, internal,[1,2] turbulent and transonic flows.[2,7,8]

In its final form, the present formulation has some features similar to the velocity split technique due to Dodge and Lieber[3]; however, this resemblance is only superficial. In the present analysis, a composite representation of inviscid and viscous region velocities is prescribed in the spirit of matched asymptotic expansions. The complete Navier-Stokes equations are solved. No simplifying approximations are required. The finite difference form of the resulting equations is solved by a coupled strongly implicit procedure described previously by the authors.[4]

Presented as Paper 82-0099 at the AIAA 20th Aerospace Sciences Meeting, Orlando, Fla., Jan. 11-14, 1982; submitted Aug. 2, 1982; revision received Feb. 1, 1983.

*Associate Professor, Department of Engineering and Applied Mechanics.

†Professor and Head, Department of Aerospace Engineering and Applied Mechanics.

Governing Equations

The governing Navier-Stokes equations in orthogonal curvilinear coordinates are:

Continuity

$$(\rho h_2 h_3 u)_\xi + (\rho h_1 h_3 v)_\eta = 0 \tag{1}$$

ξ momentum

$$\frac{\rho u}{h_1} u_\xi + \frac{\rho v}{h_2} u_\eta + \frac{\rho uv}{h_1 h_2} h_{1_\eta} - \frac{\rho v^2}{h_1 h_2} h_{2\xi} = -\frac{1}{h_1} p_\xi + \frac{1}{h_1 h_2 h_3}\left[\frac{\partial}{\partial \xi}(h_2 h_3 \tau_{11}) + \frac{\partial}{\partial \eta}(h_1 h_3 \tau_{12})\right] + \tau_{12}\frac{h_{1\eta}}{h_1 h_2} - \tau_{22}\frac{h_{2\xi}}{h_1 h_2} - \tau_{33}\frac{h_{3\xi}}{h_1 h_3} \tag{2}$$

η momentum

$$\frac{1}{h_2} p_\eta = -\frac{\rho u}{h_1} v_\xi - \frac{\rho v}{h_2} v_\eta - \frac{\rho uv}{h_1 h_2} h_{2\xi} + \frac{\rho u^2}{h_1 h_2} h_{1\eta} + \frac{1}{h_1 h_2 h_3}\left[\frac{\partial}{\partial \xi}(h_2 h_3 \tau_{12}) + \frac{\partial}{\partial \eta}(h_1 h_3 \tau_{22})\right] + \frac{\tau_{12}}{h_1 h_2} h_{2\xi} - \frac{\tau_{11}}{h_1 h_2} h_{1\eta} - \frac{\tau_{33}}{h_2 h_3} h_{3\eta} \tag{3}$$

Energy

$$\frac{\rho u}{h_1} H_\xi + \frac{\rho v}{h_2} H_\eta = \times \frac{1}{h_1 h_2 h_3}\left[\frac{\partial}{\partial \xi}(h_2 h_3 q_1) + \frac{\partial}{\partial \eta}(h_3 h_1 q_2)\right] + \Phi \tag{4}$$

State

$$\rho = p/RT \tag{5}$$

where

$$\tau_{11} = 2\mu\left[\frac{1}{h_1}\frac{\partial u}{\partial \xi} + \frac{v}{h_1 h_2}\frac{\partial h_1}{\partial \eta}\right] - \frac{2}{3}\mu\frac{1}{h_1 h_2 h_3} \times \left[\frac{\partial}{\partial \xi}(h_2 h_3 u) + \frac{\partial}{\partial \eta}(h_3 h_1 v)\right]$$

$$\tau_{22} = 2\mu\left[\frac{1}{h_1}\frac{\partial v}{\partial \xi} + \frac{u}{h_1 h_2}h_{1\xi}\right] - \frac{2}{3}\mu\frac{1}{h_1 h_2 h_3} \times \left[\frac{\partial}{\partial \xi}(h_2 h_3 u) + \frac{\partial}{\partial \eta}(h_3 h_1 v)\right]$$

$$\tau_{33} = 2\mu\left[\frac{u}{h_3 h_1}h_{3\xi} + \frac{v}{h_2 h_3}h_{3\eta}\right] - \frac{2}{3}\mu\frac{1}{h_1 h_2 h_3} \times \left[\frac{\partial}{\partial \xi}(h_2 h_3 u) + \frac{\partial}{\partial \eta}(h_3 h_1 v)\right]$$

$$\tau_{21} = \tau_{12} = \mu\left[\frac{h_2}{h_1}\frac{\partial}{\partial \xi}\left(\frac{v}{h_2}\right) + \frac{h_1}{h_2}\frac{\partial}{\partial \eta}\left(\frac{u}{h_1}\right)\right]$$

$$q_1 = \frac{1}{h_1}k\frac{\partial T}{\partial \xi}, \quad q_2 = \frac{1}{h_2}k\frac{\partial T}{\partial \eta}, \quad \mu, \quad k \propto T$$

and u and v are the components of velocity along (ξ) and normal (η) to the surface, ρ is the density, p the pressure, H the stagnation enthalpy, and Φ a dissipation function. μ and k are the coefficients of viscosity and heat conduction. h_1, h_2, and h_3 are the metrics associated with the curvilinear coordinate system. These are determined by the mapping procedure which generates the body-fitted coordinates (ξ, η) from the physical Cartesian coordinates (x,y), where $h_2 = \bar{h}_2(x,y) = h_2(\xi,\eta)$, $h_1 = \bar{h}_1(x,y) = h_1(\xi,\eta)$, and for the axisymmetric flow considered here, $h_3 = y = y(\xi,\eta)$.

Mapping Procedure

A variety of techniques for prescribing body-fitted coordinate systems is available in literature. In the present paper a conformal representation ($h_1 = h_2$) is utilized for the generation of the coordinate system, although more general orthogonal systems are acceptable. It should be emphasized that an orthogonal body-fitted coordinate system is important for the applicability of the present boundary-layer relaxation technique. In this system of coordinates, the two-dimensional inviscid incompressible flow is obtained exactly. More important, however, for the present analysis, is the fact that in these coordinates, the viscous boundary layer near the body will be properly described by a single momentum equation, i.e., the ξ equation for the flow along the surface. The normal momentum equation (3), in effect, determines the pressure variations from the inviscid values. This is in conformity with boundary-layer concepts. For this coordinate system, the composite velocity representation, to be detailed in the following section, becomes a natural extension of interacting boundary-layer theory to the full Navier-Stokes equations.

An approach for generating body-fitted coordinates, due to Davis,[6] has been used in the present investigation. This method is based on a unique extension of the Schwarz-Christoffel transformation applicable to smooth surfaces. For example

$$\frac{dz}{d\zeta} = M\exp\left[\frac{1}{\pi}\int \log(\zeta - b)\, d\beta\right], \quad z = x + iy \quad \zeta = \xi + i\eta \tag{6}$$

where the z plane is the physical plane and ζ the transformed plane. M is a parameter. A finite number of discontinuities in the body shape can easily be incorporated in the mapping routine. In the case of a boattail, one juncture point represents such a discontinuity. The nonlinear integrodifferential equation is integrated numerically. Equation (6) is rewritten as:

$$\frac{dz}{d\zeta} = f_1(\zeta) f_2(\zeta) \tag{7}$$

where $f_2(\zeta)$ is a smooth and well-behaved function and $f_1(\zeta)$ is written as $f_1(\zeta) = (\zeta - a_1)^{-1/\pi}$ near the corner points a_1. Away from the juncture $f_1(\zeta)$ is well behaved along the boattail. Equation (7) is integrated numerically between any two grid points (ζ_{i-1}, ζ_i) by using the trapezoidal rule in the complex plane. Thus,

$$z_i - z_{i-1} = f_1\left(\frac{\zeta_i + \zeta_{i-1}}{2}\right) f_2\left(\frac{\zeta_i + \zeta_{i-1}}{2}\right)(\zeta_i - \zeta_{i-1}) \tag{8a}$$

If $\zeta_{i-1} < a_1 < \zeta_i$

$$z - z_{i-1} = f_2\left(\frac{\zeta_i + \zeta_{i-1}}{2}\right)\left[\frac{(\zeta_i - a_1)^{1-1/\pi} - (\zeta_{i-1} - a_1)^{1-1/\pi}}{1 + 1/\pi}\right] \tag{8b}$$

clearly expression (8b) is well behaved near the corner singularity for a_1. A typical solution for the boattail is depicted in Fig. 1. It should be noted that the accuracy of the mapping is determined solely by the integration formula used for the integration of Eq. (7). Typically the trapezoidal rule leads to second-order accurate mapping functions and derivatives. Higher-order quadrature rules, such as Simpson's rule or the one obtained from the application of spline interpolation, also can be used when necessary. In spite of the fact that z is well behaved at $\zeta = a_1$, the mapping is nonanalytic at the boattail juncture. This introduces a considerable amount of complication in the flowfield computation. The choice of the grid in the juncture region becomes highly critical. Mesh points very close to the juncture introduce large mapping derivatives, thereby increasing the truncation error. A coarse grid may not resolve the recirculation region properly. This suggests that a proper balance between those two conflicting effects must be considered for the accurate evaluation of the boattail flowfield. The metric

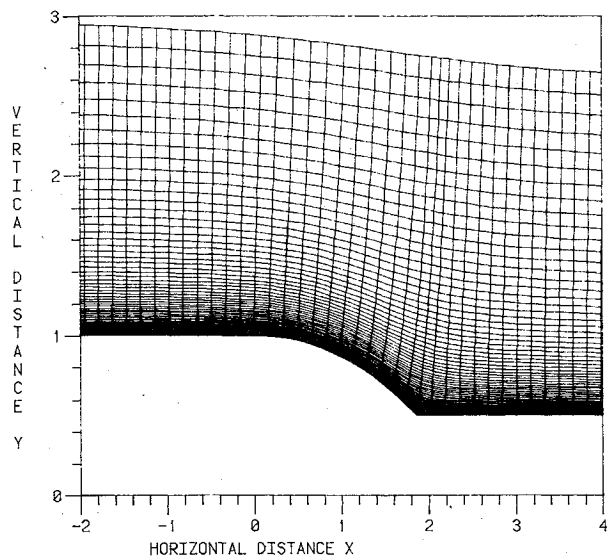

Fig. 1 Boattail grid (chord angle = 15 deg).

coefficient h_1 has been evaluated near the surface of the body by a central finite difference approximation. This introduces a certain degree of smoothing of the corner singularity.

Composite Formulation

The flow outside the thin viscous region near the surface is essentially inviscid and can be determined by a potential function ϕ; therefore, the following composite representation of the velocity field in the spirit of matched expansions is prescribed.

$$u=(U/h_1)(1+\phi_\xi)=u_eU \tag{9a}$$

$$v=(1/h_2)\phi_\eta \tag{9b}$$

These expressions are used in the Navier-Stokes equations [Eqs. (1-4)]. After some manipulation, the following system for ϕ, U, S results.

$$\left[\rho h_3\frac{h_2}{h_i}U(1+\phi_\xi)\right]_\xi+\left(\rho h_3\frac{h_i}{h_2}\phi_\eta\right)_\eta=0$$

(continuity) (10)

$$\rho\frac{\partial u}{\partial t}+\frac{1}{h_1h_2h_3}\{[\rho h_2h_3u_e^2(U^2-U)]_\xi+[\rho h_3h_1u_ev(U-1)]_\eta\}+\rho\frac{h_{1_\eta}}{h_1h_2}[u_ev(U-1)]_\eta+\rho\frac{u_e}{h_1}(U-1)u_{e_\xi}=-\frac{\rho}{h_1}G_\xi+\frac{\rho T}{h_1}S_\xi$$

+ viscous terms (ξ momentum) (11)

$$TS_\eta=G_\eta+(U-1)\left[\left(\frac{u_e^2}{2}\right)_\eta-\frac{h_{1_\eta}}{h_1}u_e^2U\right]$$

+ viscous terms (η momentum) (12)

where

$$G=\frac{\gamma}{\gamma-1}\frac{p}{\rho}+\frac{u_e^2+v^2}{2}-\bar{G}(\xi) \tag{13}$$

$$p=\text{const}\ \rho^\gamma\exp[\gamma(\gamma-1)M_\infty^2S]$$

and $\bar{G}(\xi)$ is specified for external flow so that $G=0$ in the freestream. G is similar to a Bernoulli or total pressure in the inviscid region and S is proportional to the entropy. It is chosen to be zero in the freestream. G is not assumed constant, but is determined by the calculation procedure. In the inviscid region $U\to1$ and the continuity equation reduces to the familiar nonlinear potential flow equation. The momentum equations are satisfied identically with $G=$ const. In the viscous region, the continuity and ξ-momentum equations determine U and ϕ. The viscous total pressure correction is obtained from the η-momentum equation in which only η derivatives appear. These two flow regions, pertinent to large Reynolds number analysis, are then appropriately described by the composite system [Eqs. (10-13)]. The equations conform with those of boundary-layer and inviscid flow theory.

This method of defining v with a "potential" was first tested for the flat plate boundary-layer (U,ϕ) equations. The solution of the resulting two-point boundary-value problem exactly reproduced the results obtained with standard methods based on the velocities u and v. It should be noted that the present system of equations can also be used for the solution of the inviscid flow when $Re=\infty$ and $U=1$ on the surface. With $S_\xi\equiv0$ in Eq. (11), the normal momentum equation (12) decouples from the axial momentum equation (11) and continuity equation (10); therefore, the system (11-12) represents an interacting boundary-layer approximation, if axial diffusion terms are neglected. In addition, if ϕ_ξ and $\phi_{\xi\xi}$ in Eqs. (10) and (11) are replaced with their respective potential flow values, the usual boundary-layer approximation is recovered.

For the calculations of separated flows it is essential that U and ϕ be solved in a coupled fashion to eliminate the pressure singularity that would otherwise occur at the separation point. However, the variable G, which represents the Bernoulli constant in the inviscid flow, can be treated explicitly. Finally, the η-momentum equation (12) determines the entropy, S, variation across the viscous layer, and when combined with the energy equation and the equation of state leads to ρ, T, and p. The coupling between U and ϕ is maintained with the coupled strongly implicit procedure (CSIP)[4] for the solution of the algebraic system obtained by discretizing Eqs. (10) and (11).

Dodge and Lieber[3] have considered a velocity-split procedure in which $u=U+\phi_x$, $v=V+\phi_y$, where ϕ is evaluated from the inviscid flow alone. This splitting introduces an extra unknown, i.e., $(u,v)\to(U,V,\phi)$, so that an auxiliary condition is required. This is introduced by assuming that the pressure is determined from the potential ϕ alone, i.e., the "inviscid" Bernoulli equation. Also, V is determined from the η-momentum equation and not the continuity equation, as for the composite and boundary-layer procedures. More important is the fact that this splitting is not a true composite representation of the inviscid and viscous flows, since the overlap solution is not included, i.e., $u=u_{\text{INV}}+u_{\text{VIS}}-u_{\text{OVERLAP}}$. This creates considerable difficulty with boundary conditions and reflects on the "numerical matching" of the U, V, ϕ system. In the composite approach presented herein, the boundary conditions are obtained in a straightforward and natural manner. The matching of U, ϕ is consistent with the asymptotic theory.

Finally, the Dodge procedure has experienced difficulty for separated flows; a problem not encountered with the (U,ϕ) composite formulation.

Boundary Conditions

Since the geometry under consideration is infinite in both directions, the inflow and outflow conditions are extremely important for the solution of the flow problem. At the inflow, $\xi=0$, $U=1$, $\phi=0$, $H=H_e$, except at $\eta=0$, where $U=0$, $H=H_w$. On the solid surface, $\eta=0$, $U=\phi_\eta=0$, and for $\eta\to\infty$, $U\to1$, $\phi\to0$, $H\to H_e$, $S\to0$. At the outflow, $\xi\to\infty$, $U_{\xi\xi}=0$, and $\phi_\xi=0$. In effect, the latter outflow condition eliminates the viscous-inviscid interaction within the boundary layer.

Solution Procedure

The governing equations have been discretized using second-order accurate central differencing for all ξ derivatives except the $(\rho h_3U)_\xi$ term in the continuity equation; this term, which vanishes in the inviscid flow, is backward differenced. The η derivatives are also central differenced, except for the normal momentum equation (12), for which the two-point trapezoidal rule is applied. The resulting implicit algebraic system of equations has been solved iteratively using the coupled strongly implicit procedure. The continuity and ξ-momentum equations for ϕ and U are solved in a coupled fashion, while the η-momentum equation for S is evaluated iteratively. The energy equation is solved independently with the strongly implicit algorithm. In the ξ-momentum equation, G and S are treated as known during each iteration. Although the total pressure G is evaluated explicitly from the energy equation, the static pressure is completely unknown and depends upon the values of ϕ_ξ and ϕ_η. Since ϕ is evaluated implicitly in the coupled algorithm, this implies that the

pressure is also treated implicitly. This procedure eliminates the separation singularity. Also, in view of the relaxation nature of the method of solution, i.e., $\phi_{\xi\xi}$ terms in Eqs. (10) and (11), departure solutions, typical of marching techniques, do not appear.

Coupled 2×2 Solution Algorithm

In an earlier paper[4] the present authors developed a coupled strongly implicit procedure for the stream function-vorticity form of the Navier-Stokes equations. This algorithm has the distinct advantages of being implicit in both the ξ and η directions, as well as allowing for the coupling of all the boundary conditions. Furthermore, the method is unconditionally stable, allows for arbitrarily large Δt, converges faster than SOR, LSOR, ADI, etc., and is insensitive to the grid aspect ratio. The discretized version of the equations can be written as

$$(A+P)\,V_n^{n+1} = G + PV^n$$

where

$$V = \begin{bmatrix} U_{ij} \\ \phi_{ij} \end{bmatrix}, \quad U_{ij} = \begin{bmatrix} u_{1_j} \\ u_{2_j} \\ \vdots \\ u_{NJ} \end{bmatrix}, \quad \phi_{ij} = \begin{bmatrix} \phi_{1_j} \\ \phi_{2_j} \\ \vdots \\ \phi_{NJ} \end{bmatrix}$$

P is chosen such that $(A+P)$ can be decomposed into a lower and upper triangular form having a sparsity pattern similar to the original matrix A. This leads to a solution algorithm of the following form

$$\begin{bmatrix} U_{ij} \\ \phi_{ij} \end{bmatrix}^{n+1} = \begin{bmatrix} GM_{1_{ij}} \\ GM_{2_{ij}} \end{bmatrix} + \begin{bmatrix} T_{1_{ij}} & T_{3_{ij}} \\ T_{5_{ij}} & T_{7_{ij}} \end{bmatrix} \begin{bmatrix} U_{i,j-1} \\ \phi_{i,j-1} \end{bmatrix}^{n+1} + \begin{bmatrix} T_{2_{ij}} & T_{4_{ij}} \\ T_{6_{ij}} & T_{8_{ij}} \end{bmatrix} \begin{bmatrix} U_{i-1,j} \\ \phi_{i-1,j} \end{bmatrix}^{n+1}$$

where n is the iteration index. Although the coupling accelerates the rate of convergence, it also increases the storage requirement by a factor of two. In its present form the CSIP is slightly different from the one given in Ref. 4. The forward and backward sweeps have been reversed in order to impart a certain degree of marching, consistent with the boundary-layer behavior. As shown in Ref. 4, the appropriate recurrence relationships can easily be obtained.

Results

Both unseparated and separated flows are considered. As a simple but important test of the procedure, the laminar flow along an infinite straight cylinder at zero incidence for $Re=7500$ and a variety of subsonic Mach numbers were evaluated. The results are in excellent agreement with the known boundary-layer solutions. In the present paper, the results for subsonic flow along a boattail geometry are presented. The boattail shown in Fig. 1 consists of a circular-arc section which joins the cylinder at an angle of 15 deg. This is the chord angle from the onset of the boattail to the juncture. The local corner angle is 30 deg. The boattail is mapped into an infinite cylinder using the Schwarz-Christoffel transformation. Of the 60 equally-spaced points along the boattail in the physical plane, 12 are along the circular-arc section. The computational grid in the physical plane is shown in Fig. 1. Although the solution procedure did not have any problems near the corner of the boattail, the pressure and skin friction, as shown in Figs. 2a and 2b, exhibit kinks due to the singularity in the transformation when the metric h_1 was

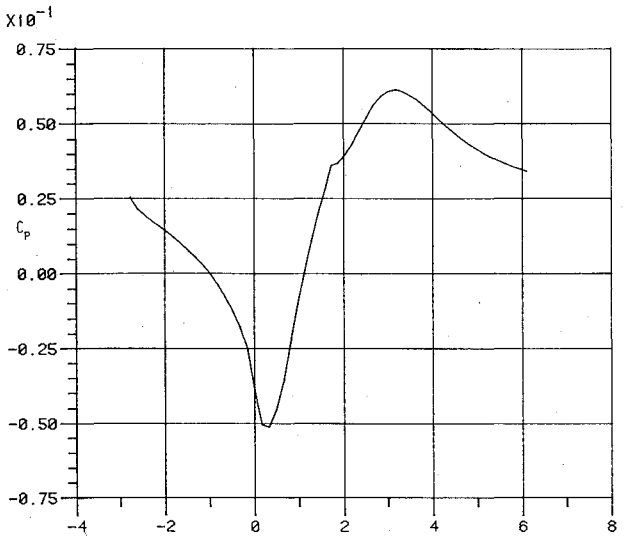

Fig. 2a Pressure coefficient, $Re=1500$, $M_\infty=0.3$.

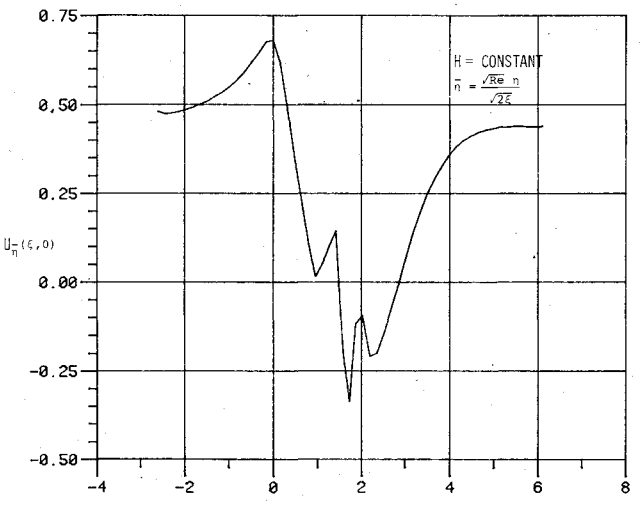

Fig. 2b Skin friction parameter, $Re=1500$, $M_\infty=0.3$.

calculated analytically. This behavior is further amplified with coarse grids. Smoother solutions are obtained with finer grids and by using finite difference approximations for the calculations of h_1. With improved resolution these can be suppressed. As noted previously, this amounts to smoothing the corner region. Since the geometry under investigation is infinite and a discontinuous (step) inflow solution for U is prescribed, the inflow location behaves very much like a leading edge. In order to avoid any computational problems associated with this approximate initial condition, a boundary-layer approximation was imposed for the first five grid points in both the ξ and η directions, i.e., $G_\xi - TS_\xi = 0$.

Figure 3 depicts the streamlines over the boattail for $Re=5000$, $M_\infty=0.8$ and $Re=7500$ and $M_\infty=0.3$. In all the cases considered, an inviscid flow was first evaluated by prescribing $U=1$ on the body surface. Uniform initial conditions for U were assumed for the inviscid calculation. For the first 50 steps of the iterative cycle a time increment $\Delta t=0.1$ was prescribed. Subsequently, Δt was increased to 10^6. The final solutions are obtained with this value of Δt. For $Re<2000$ and $M_\infty<0.3$, it was possible to start with $\Delta t=10^6$ directly. This may perhaps be a fortuitious circumstance associated with the relatively coarse grid that has been specified for the present investigation. For finer grids, it is not expected that large Δt values can be used in the initial stages of the transient. The pressure coefficient and skin friction along the surface are shown in Figs. 4 and 5, respectively. These

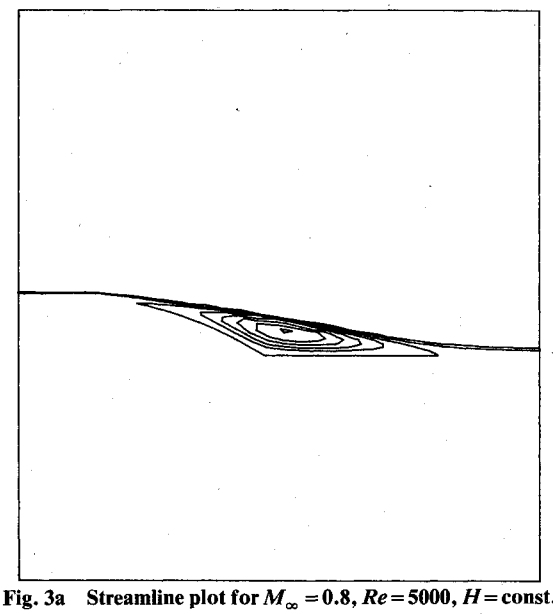

Fig. 3a Streamline plot for $M_\infty = 0.8$, $Re = 5000$, $H = \text{const.}$

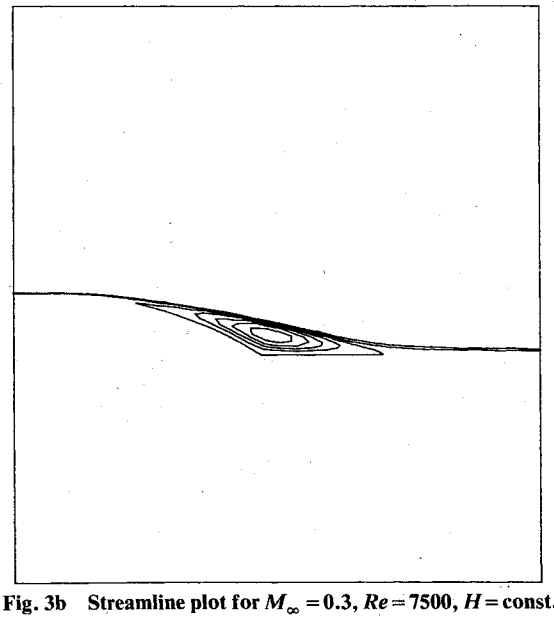

Fig. 3b Streamline plot for $M_\infty = 0.3$, $Re = 7500$, $H = \text{const.}$

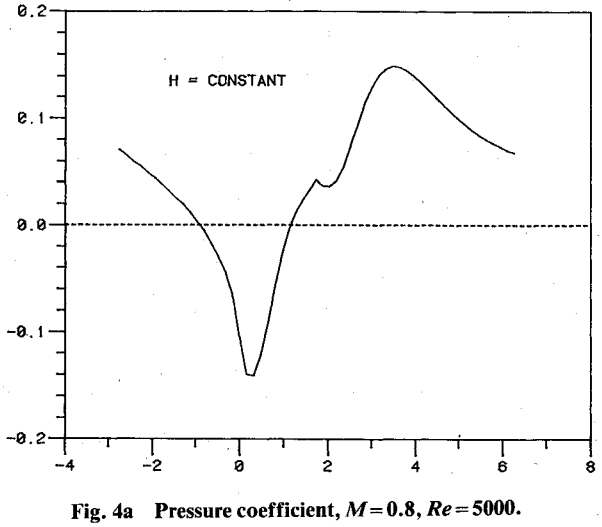

Fig. 4a Pressure coefficient, $M = 0.8$, $Re = 5000$.

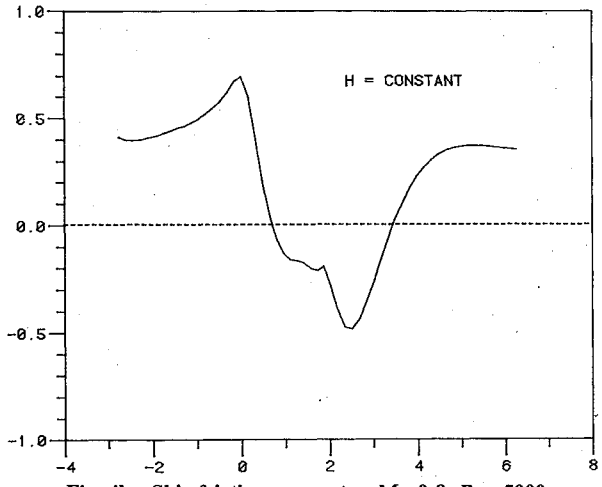

Fig. 4b Skin friction parameter, $M = 0.8$, $Re = 5000$.

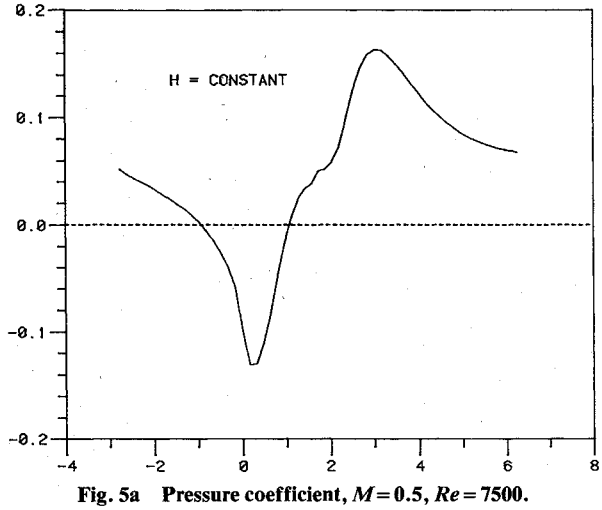

Fig. 5a Pressure coefficient, $M = 0.5$, $Re = 7500$.

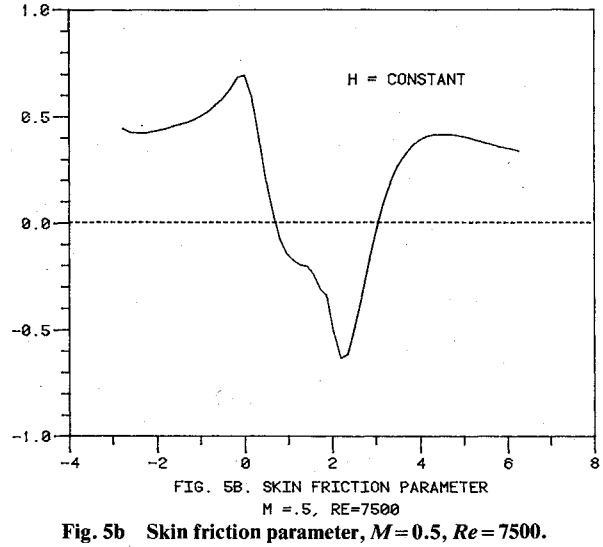

Fig. 5b Skin friction parameter, $M = 0.5$, $Re = 7500$.

results are for constant stagnation enthalpy [$H = 1 + (\gamma - 1)/2M_\infty^2$]. As the Reynolds number increases the separation point moves upstream, i.e., towards the beginning of the boattail. The size of the recirculation bubble increases from 2.2 rad for $Re = 5000$ and $M_\infty = 0.3$ to 2.3 rad for $Re = 7500$, $M_\infty = 0.3$ and to 2.7 rad for $Re = 5000$ and $M_\infty = 0.8$. The peak pressure generally occurs about one grid point downstream of the reattachment point.

Solutions for a cold wall boundary conditions corresponding to $H_w = 0.85\ H_\infty$, $Re = 7500$, and $M_\infty = 0.5$ are

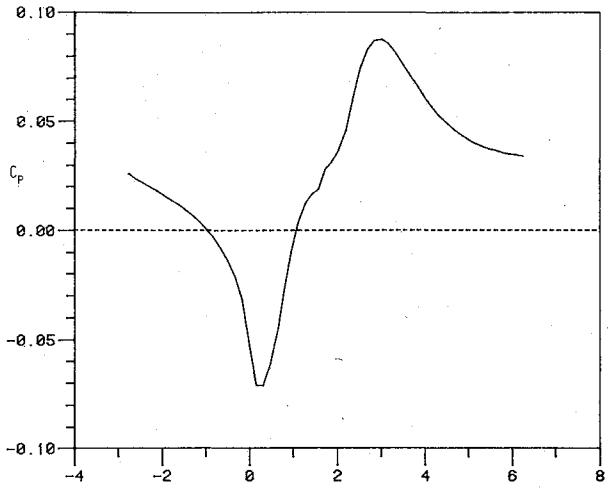

Fig. 6a Pressure coefficient, $M_\infty = 0.5$, $Re = 7500$, $H_w = 0.85\, H_\infty$.

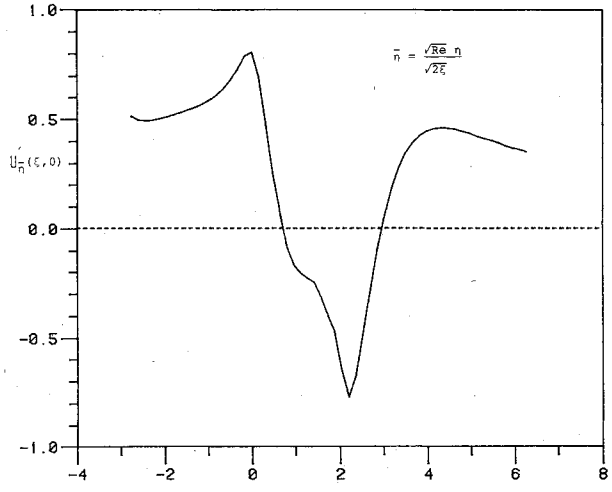

Fig. 6b Skin friction parameter, $M_\infty = 0.5$, $Re = 7500$, $H_w = 0.85\, H_\infty$.

shown in Fig. 6. It should be noted that the effect of this cold wall boundary condition on the final solution is minimal. Finally, solutions have been obtained for $Re = 10^4$, $M_\infty = 0.3$. As the Reynolds number increases, mesh refinement and therefore smaller initial values of Δt are required. In addition, a Khosla-Rubin (K-R)[5] type of deferred-corrector for $(\rho h_3 U)_\xi$ is helpful during the transient phase, allows for larger values of Δt, and provides better stability and convergence characteristics. Furthermore, it should be pointed out that for the cases under consideration, step initial conditions ($u = 1$, $v = 0$, $y > 0$; $u = v = 0$, $y = 0$) are prescribed at approximately 3 rad upstream of the boattail. The flow negotiating the turn exhibits a relatively thin boundary layer with a steep velocity profile. This initial condition has a significant influence on and limits the extent of the recirculation region. The effect of inflow conditions on the flow characteristics on the boattail can be substantial and this effect is considered in greater detail in Ref. 8.

All of the computations have been carried out on the University of Cincinnati Amdahl V470 computer. Typical CPU time for a converged solution with 60×30 grid is approximately 15 min. The computational domain starts approximately 3 rad upstream of the boattail and terminates at 6 rad downstream. The outer (η) boundary is at 13 rad.

Summary

A new solution procedure based on a composite velocity representation suitable for high Reynolds number compressible viscous flows is considered herein. The method reduces to a potential flow description in an inviscid region and in viscous layers represents the extension of viscous-inviscid interacting boundary-layer theory to the complete Navier-Stokes equations. A CSIP is used to couple the viscous U and inviscid ϕ velocity components. This algorithm is extremely efficient as a steady-state solver.

Acknowledgments

Thanks are due to Prof. R. T. Davis for providing the Schwarz-Christoffel code for mapping the boattail geometry. This research was supported by the Propulsion Aerodynamics Branch of the NASA Langley Research Center under Grant NAG I-8.

References

[1] Rubin, S. G. and Khosla, P. K., "A Composite Velocity Procedure for the Incompressible Navier-Stokes Equations," *8th International Conference on Numerical Methods in Fluid Mechanics*, Springer-Verlag, 1982, pp. 448-454.

[2] Rubin, S. G., *Von Kármán Institute Lecture Series on Computational Fluid Dynamics*, Brussels, Belgium, 1982.

[3] Dodge, P. R. and Lieber, L. S., "A Numerical Method for the Solution of Navier-Stokes Equations for a Separated Flow," AIAA Paper 77-170, 1977.

[4] Rubin, S. G. and Khosla, P. K., "Navier-Stokes Calculations with a Coupled Strongly Implicit Method," *Comp. Fluids*, Vol. 9, No. 2, 1979, p. 163.

[5] Khosla, P. K. and Rubin, S. G., "A Diagonally Dominant Second-Order Accuate Implicit Scheme," Vol. 2, No. 2, 1974, pp. 207-210.

[6] Davis, R. T., "Numerical Methods for Coordinate Generation Based on Schwartz-Christoffel Transformations," *Proceedings of the AIAA Computational Fluid Dynamics Conference*, Williamsburg, Va., 1979, p. 180.

[7] Celestina, M., "Solution of Navier-Stokes Equations for Subsonic Turbulent Flow Over Boattail Geometry," M.S. Thesis, Dept. of Aerospace Engineering, University of Cincinnati, Ohio, 1983.

[8] Swanson, R. C., Rubin, S. G., and Khosla, P. K., "Calculation of Afterbody Flows with a Composite Velocity Formulation," AIAA Paper 83-1736, Danvers, Mass., July 1983.